

# Relativistic Reflection: Review and Recent Developments in Modeling

T. Dauser<sup>1,\*</sup>, J. García<sup>2</sup>, and J. Wilms<sup>1</sup>

<sup>1</sup> Dr. Karl Remeis-Observatory and Erlangen Centre for Astroparticle Physics, Sternwartstr. 7, 96049 Bamberg, Germany

<sup>2</sup> Harvard-Smithsonian Center for Astrophysics, 60 Garden Street, Cambridge, MA 02138, USA

Received 01 Jan 2016, accepted 15 Jan 2016

Published online 2016 Apr 25

**Key words** black hole physics, X-rays: galaxies, line: profiles

Measuring relativistic reflection is an important tool to study the innermost regions of the an accreting black hole system. In the following we present a brief review on the different aspects contributing to the relativistic reflection. The combined approach is for the first time incorporated in the new `relxill` model. The advantages of this more self-consistent approach are briefly summarized. A special focus is put on the new definition of the intrinsic reflection fraction in the lamp post geometry, which allows to draw conclusions about the primary source of radiation in these system. Additionally the influence of the high energy cutoff of the primary source on the reflection spectrum is motivated, revealing the remarkable capabilities of constraining  $E_{\text{cut}}$  by measuring relativistic reflection spectra from *NuSTAR*, preferably with lower energy coverage.

© 2016 WILEY-VCH Verlag GmbH & Co. KGaA, Weinheim

## 1 Introduction

Reflection of X-ray radiation at the innermost regions of the accretion disk is strongly distorted due to the strong effects of general relativity close to the central black hole (Fabian et al., 1989). Depending on the spin of the black hole, these distortions will transform narrow emission lines to broad, skew-symmetric features. This broadening is only apparent, however, if most of the radiation originates from the innermost regions of the accretion disk (Laor, 1991). Due to a combination of abundances and fluorescent yield, the neutral Fe  $K\alpha$  line at 6.4 keV is typically the strongest fluorescent emission line seen in AGN and GBH spectra. First hints that the fluorescent iron line originates from reflection of X-ray radiation at a dense accretion disk were obtained by Barr et al. (1985) for Cygnus X-1 and in AGN by Nandra et al. (1989) and Pounds et al. (1990). The broadening effect of this iron line due to the vicinity of the reflector to the black hole was already predicted by a number of studies (see, e.g., Fabian et al., 1989; Matt et al., 1991, 1992; Stella, 1990), while the data was still not able to constrain these models (Mushotzky et al., 1993). Finally, Tanaka et al. (1995) analyzed a long *ASCA* observation of MCG–6-30-15 and concluded that the skew-symmetric broad emission line present in the spectrum originates from reflection only a few gravitational radii away from the central black hole. Further studies have revealed that a large number of AGN show a broadened iron line (Guainazzi et al., 2006; Longinotti et al., 2008; Nandra et al., 2007; Patrick et al., 2011). With the advent of high signal-to-noise observations (e.g., from *XMM-Newton*, *Suzaku*, or *NuS-*

*TAR*) not only a single broadened line could be observed, but instead the complete reflection spectrum of the accretion disk was required to be relativistically distorted. Those techniques lead to the detection of relativistic reflection features in many AGN, such as, e.g., MCG–6-30-15 (Fabian & Vaughan, 2003; Marinucci et al., 2014; Wilms et al., 2001), 1H0707–495 (Dauser et al., 2012; Fabian et al., 2009), or NGC 1365, (Risaliti et al., 2013), Galactic Black Holes, such as Cyg X-1 (Duro et al., 2011; Fabian et al., 1989; Tomsick et al., 2014), GRS 1915+10 (Miller et al., 2013b), or GX 339–4 (Miller et al., 2008; Reis et al., 2008), and neutron stars (e.g., Serpens X-1; Miller et al., 2013a).

## 2 The Big Picture

Relativistic reflection is created by a complex interplay of effects. In the following the single contributions will be briefly summarized. From our current understanding a primary source is irradiating the accretion disk. The irradiating spectrum is then reflected, imprinting the atomic features such as abundances and ionization state of the disk into the reflected spectrum. Finally this outgoing spectrum is relativistically distorted on its way to the observer.

### 2.1 Reflection in the Rest Frame of the Accretion Disk

At first we will discuss the reflection itself, which takes place in the rest frame of the accretion disk. The model most used in the last decade for fitting relativistic reflection by applying a relativistic blurring kernel to it, is the `relionx` model (Ross & Fabian, 2005; Ross & Fabian, 2007; Ross et al., 1999). More recently, the `xillver` model (García et al., 2013; García & Kallman, 2010; García et al., 2011)

\* Corresponding author: e-mail: thomas.dauser@fau.de

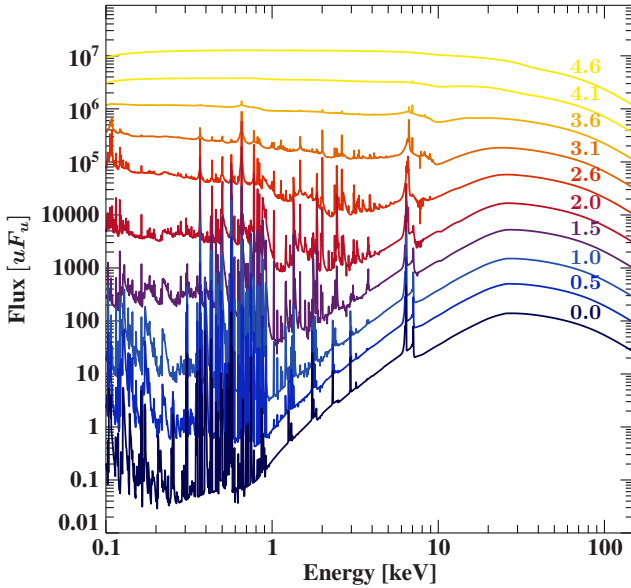


**Fig. 1** Reflection spectra calculated with the `xillver` model (García et al., 2013; García & Kallman, 2010; García et al., 2011) for different values of the ionization parameter  $\xi$ , assuming a constant density of the accretion disk ( $n = 10^{-15} \text{ cm}^{-3}$ ). The values in the plots specify  $\log \xi$  for each curve, from a neutral disk ( $\log \xi = 0$ ) to a completely ionized disk ( $\log \xi = 4.6$ ). Note that the spectra are not renormalized, but instead the flux scales linearly with the ionization parameter for constant density.

was developed. It uses a similar approach with an extended set of atomic data. Both models are largely in agreement. The major improvement of `xillver` comes from the usage of the largest collection of atomic data in X-ray astronomy, namely the `xstar`<sup>1</sup> atomic database (Bautista & Kallman, 2001). One important difference between these models concerns the assumptions made on the effect of resonant scattering and subsequent Auger destruction. In `reflionx`, it is assumed that this effect completely suppress the emission of Fe K lines for second row ions (i.e., Fe XVII-XXII). In `xillver`, the branching ratios for Auger versus fluorescence emission are explicitly calculated, and significant line emission is still observed after the effects of Auger decay are included. Thus, in the range of ionization where these ions are most predominant ( $2 \lesssim \log \Xi \lesssim 3$ ), the two models are highly discrepant, with `reflionx` exhibiting very small Fe K emission compared to `xillver`.

Figure 1 shows ionized reflection spectra for different ionizations of the accretion disk. The ionization is parametrized by the ionization parameter  $\xi$ , which is defined as the incident flux  $F$  divided by the density of the disk  $n$ , namely  $\xi = 4\pi F/n$ . A low value implies that the disk is almost neutral ( $\xi \sim 1$ ). As can be seen in the figure, this leads to a strong Fe K $\alpha$  line at 6.4 keV and a large forest of emission and absorption lines at lower energies. For

increasing ionization parameter, the number and strength of these lines generally decreases, leading to what is called a highly ionized disk for  $\xi = 10^3$ . For even larger values of ionization ( $\xi = 10^4$ ), the disk is fully ionized. This means that the disk acts almost as a mirror and therefore the spectrum exhibits no line features (see García et al., 2013, for a more detailed description). It is notable that the most prominent feature, the iron K $\alpha$  line at roughly 6.4 keV, strongly changes in shape and flux for different ionizations  $\xi$ .

## 2.2 Relativistic Smearing

The reflection spectrum as described in the previous section will then get relativistically distorted on its way to the observer. Various models have been developed in the past to describe the shape of the relativistically smeared features (e.g., `diskline`, `laor`, `kyrline`, `kerrdisk`, or `relline`, as published in Fabian et al., 1989; Laor, 1991; Dovčiak et al., 2004; Brenneman & Reynolds, 2006; Dauser et al., 2010, respectively.) All these models predict the relativistic line profile for a narrow line emitted in the rest frame of the accretion disk. Depending on the parameters of the system, such as for example the spin, the irradiation of the disk, or the inclination to the system the relativistic distortion then leads to different line shapes. Due to the gravitational redshift and the motion of the emitting particles in the disk, these lines are always broadened. The actual shape of these lines strongly depends on the parameters of the black hole system. Generally, a higher spin leads to broader reflection features, as can be seen in Fig. 2. This is due to the fact that for larger values of spin the accretion disk extends closer to the black hole and therefore more highly redshifted photons from these innermost parts are emitted. But also other parameters such as the inclination angle or the emissivity profile, which is the irradiating intensity impinging on the disk, lead to significant differences in shape.

## 2.3 Irradiation of the Accretion Disk

Most importantly, as shown in Dauser et al. (2013), the irradiating primary source also strongly influences the broadening of the line shape. In general terms, it determines how important the highly relativistic inner parts of the disk contribute to the total reflection spectrum. While a low source height leads to a strong focusing of the photons onto the inner regions and therefore a broad feature, a large source height irradiates a much larger part of the disk more constantly and therefore renders the line shape to be narrower.

In the canonical coronal model of the  $\alpha$  disk (Shakura & Sunyaev, 1973), the radial intensity is given by  $I \propto r^{-3}$ . However, generally emissivities much steeper at small radii are observed (see, e.g., Dauser et al., 2012; Fabian et al., 2004; Miller et al., 2013b; Risaliti et al., 2013; Wilms et al., 2001). The lamp post geometry, in which the primary source is above the black hole on the rotational axis of the black hole, automatically predicts such steep emissivities. These considerations are strengthened by direct measurements of

<sup>1</sup> See <http://heasarc.gsfc.nasa.gov/xstar/xstar.html> for more information.

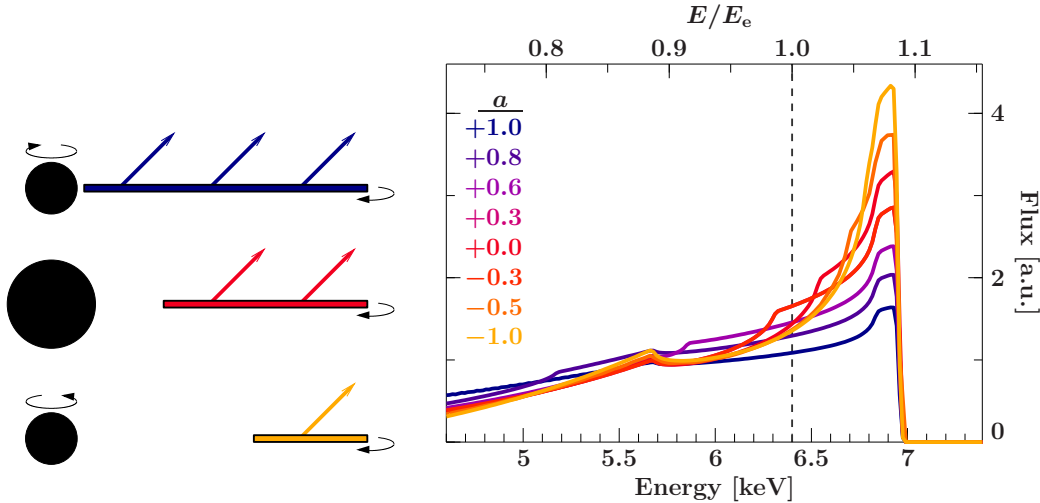


**Fig. 2** *Left:* sketch of the black hole and the accretion disk for high, zero, and negative spin (from top to bottom). The inner edge of the disk is moving outwards for decreasing spin. Note that the size of the black hole changes with its spin. *Right:* line profiles for the different values of spin.

the emissivity profile (see Wilkins & Fabian, 2012). Note that the shape of the primary source is likely not point-like as assumed in the simple lamp post geometry, but probably extended (see Wilkins & Gallo, 2015).

Independent of the origin of the primary radiation, the extent of relativistic broadening of the reflection features already allows to draw conclusions. Namely, the broad features can only be created by a primary source emitting the majority of its radiation below  $10 r_g^2$  (Fabian et al., 2014). The fact that the primary source is very compact and close to the black hole is also supported by spectral-timing and reverberation studies (Cackett et al., 2014; Kara et al., 2013; Uttley et al., 2014).

In the following we present a more self-consistent approach to modeling relativistic reflection, by focusing on its advantages and new features.

### 3 Self-consistent Modeling of Relativistic Reflection

The `relxill` model<sup>3</sup> was implemented in order to directly combine the previously described steps of irradiation, reflection, and relativistic smearing. This approach has several important advantages, as has been extensively described and analyzed in García et al. (2014). It uses the `xillver` model for the non-relativistic reflection (described in Sect. 2.2) and the `relline` kernel for the relativistic blurring.

The most important change is that the new model allows for the first time to take the angular directionality in a relativistic reflection spectrum into account. As is described in

detail in García et al. (2014) this means that instead of taking an angle averaged spectrum for the complete accretion disk, now each point of the disk gets the proper reflection spectrum for the emission angle as seen by the distant observer. Note that due to strong gravitational light-bending effects this emission angle often strongly differs from the inclination angle, which necessitates the chosen approach.

As also presented in García et al. (2014), the direct consequence of the change in spectrum is that important system parameters like the spin and the inclination angle are better constrained by the `relxill` model. The actual values of those parameters is mainly consistent with the previous, angle-averaged approach. Solely we could show that the iron abundance might have been over-estimated by up to a factor of two.

Besides the direct consequences of the self-consistent model by taking the angular directionality into account, the combined approach of the `relxill` model does have additional important advantages. In the following we will briefly focus on the reflection fraction as a new, intrinsic parameter (Sect. 3.1) and the possibility to constrain coronal parameters by exploiting the strong influence of the high energy cutoff on the reflection spectrum (Sect. 3.2).

#### 3.1 The Reflection Fraction

The `relxill` model allows for the possibility to predict the direct and reflected spectrum simultaneously. While strictly speaking no improvement in the spectral model itself, this combination has important consequences by allowing to fit directly for the reflection fraction  $R_f$ . This reflection fraction, which characterizes the strength of the reflection, can be used as a measure for the accretion geometry. As shown in Dauser et al. (2014), it also allows for stricter constraints on the spin of the black hole, as high values of

<sup>2</sup>  $r_g = GM/c^2$  is the gravitational radius

<sup>3</sup> Can be downloaded at <http://www.sternwarte.uni-erlangen.de/research/relxill/>

the reflection fraction are only possible for a rapidly rotating black hole.

### 3.1.1 Definition

Formally, the reflection fraction is defined in terms of the fraction of emitted photons of the primary source which will hit the accretion disk ( $N_{\text{AD}}$ ) compared to the fraction of photons escaping to infinity ( $N_{\infty}$ ):

$$R_{\text{f}} = \frac{N_{\text{AD}}}{N_{\infty}} \quad (1)$$

In order to consistently calculate these fractions, a certain geometry has to be assumed. In the case of the lamp post geometry, these fraction have been calculated in a ray tracing simulation as described in Dauser et al. (2014).

The important fact about this definition of the reflection fraction is that it is not simply the ratio of observed fluxes, but it is intrinsic to the black hole system. Therefore we can directly measure the fraction of photons hitting the accretion disk, making it possible to put constraints on the geometry of the system. Such an intrinsic definition is currently only available for the lamp post geometry (i.e., the `relxilllp` model). As motivated in Sect. 2.3, however, the lamp post geometry seems to be a good description for the primary source in the observed sources.

The reflection fraction of the normal `relxill` model, which does not assume a certain geometry, is defined by simply taking the ratio of the reflected flux to the direct flux in the 20–40 keV band. This energy range, coinciding with the Compton hump, is chosen as its flux is largely independent of the intrinsic parameters of the reflection such as the ionization or the abundance (see Fig. 1).<sup>4</sup> This approach, however, still does not take any relativistic boosting effects into account and therefore this value of reflection fraction might largely differ from the intrinsic definition in some cases.

### 3.1.2 Overall Flux Normalization of `relxilllp`

In order to predict the flux starting from the intrinsic reflection fraction, we need to ensure a proper normalization throughout the ray-tracing code. As flux is not directly conserved in general relativity (see Liouville's theorem), additional effort has to be taken in order to ensure this. The different steps will be briefly summarized in the following.

Such a definition of the normalization then allows to directly compare the flux for different combinations of parameters of the `relxilllp` model (e.g., for different source heights).<sup>5</sup>

<sup>4</sup> Note that this definition also differs from the one of the `pxravl` model, which uses the total reflected flux to define the reflection fraction. While being a good description for distant reflection, it is therefore not applicable for relativistic reflection.

<sup>5</sup> Feature is included since the `relxill` version v0.3a.

**Irradiation** Starting with the intensities emitted at the primary source ( $N_{\text{AD}}$  and  $N_{\infty}$ , see Eq. 1), we calculate the intensity as seen at infinity ( $I_{\infty}$ ) and at the accretion disk ( $I_{\text{AD}}$ ). In the non-relativistic limit we would expect an equal number of photons emitted towards the disk and towards infinity (i.e.,  $N_{\text{AD}} = N_{\infty}$ ).

Using the momentum and 4-velocity presented in Dauser et al. (2013), the direct radiation observed at infinity from a source at height  $h$  is then given by

$$I_{\infty} = \left( \frac{1}{u_h^t} \right)^{\Gamma} N_{\infty} = \left( \sqrt{1 - \frac{2h}{h^2 + a^2}} \right)^{\Gamma} N_{\infty} \quad (2)$$

Similarly, as calculated in Dauser et al. (2013), the incident intensity on the accretion disk is given by

$$I_{\text{AD}} = \frac{\sin \delta g_{\text{lp}}^{\Gamma}}{A(r, \Delta r) \gamma^{(\phi)}} N_{\text{AD}} \quad (3)$$

with  $\delta$  being the emission angle at the primary source,  $A$  the effective area of a ring  $\Delta r$  as seen by the incident photons,  $\gamma^{(\phi)}$  the Doppler factor, and

$$g_{\text{lp}} = \frac{(r\sqrt{r} + a) \sqrt{h^2 - 2h + a^2}}{\sqrt{r} \sqrt{r^2 - 3r + 2a\sqrt{r} \sqrt{h^2 + a^2}}} \quad (4)$$

Using these information and the fraction calculated from the incident intensity at the accretion disk and at infinity for the direct radiation are plotted in Fig. 3. Note that the normalization condition is full-filled although the curves do not converge towards 1. First of all the accretion disk in this simulation is truncated at an outer radius of  $1000 r_{\text{g}}$  and therefore for larger heights the direct flux as seen at infinity increases simply due to geometrical reasons. Moreover, it is also evident that even for large heights the total integrated flux does not add up to a value of 2, which would be expected in flat space time. The reason for this is that the energy boosting of the photons hitting the inner parts of the accretion disk increase the overall flux even for large source heights due to boosting from the energy shift<sup>6</sup>. Note that the strength of this boosting strongly depends on the steepness of the incident spectrum (see Dauser et al., 2013).

**Reflection** The flux of the incident radiation ( $I_{\text{AD}}$ ) is now used to normalized the intrinsic `xillver` spectrum. For this purpose we need the normalization of the incident spectrum, which was used to calculate the `xillver` table. As described in, e.g., García et al. (2013) it is defined as a cutoff power law with power law index  $\Gamma$  and an exponential high energy at an energy of  $E_{\text{cut}}$ . The total flux of the input radiation is set to be

$$\int_{E_{\text{lo}}}^{E_{\text{hi}}} I_{\text{incident}} = \frac{\xi n}{4\pi} \quad (5)$$

where  $E_{\text{lo}} = 0.1 \text{ keV}$ ,  $E_{\text{hi}} = 1000 \text{ keV}$ , the density  $n = 10^{15} \text{ cm}^{-2}$ , and  $\xi$  the ionization parameter.

<sup>6</sup> Photons emitted from large distances are seen strongly blue-shifted at the inner parts of the accretion disk, which also leads to a strong boost in flux

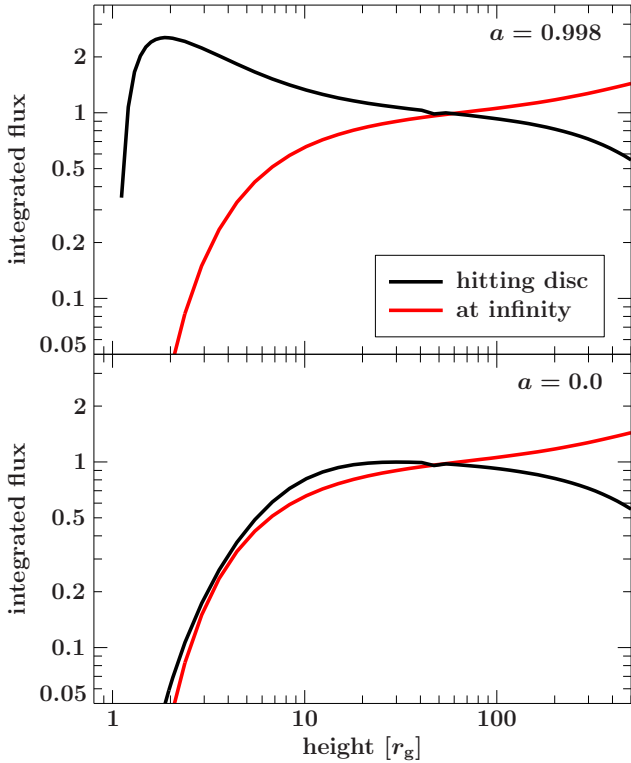


**Fig. 3** Plotted is the flux hitting the disk (black) and the flux at infinity (red). The flux at infinity is reduced at low heights due to gravitational red-shift. One can also nicely see that for low spin and low source height basically not much reflection and even less direct radiation is expected. This plot does not yet include any effects from reflection at the disk and from the disk to the observer (boosting and inclination). Note that the behavior at large heights is exactly what one would expect from an accretion disk with an outer radius of  $1000 r_g$ .

**Relativistic Smearing** As a last step, the reflection spectrum in the rest frame of the disk, which is already normalized regarding the incident flux, is relativistically smeared on its way to the observer. Intrinsically, this is achieved by the `relconv` kernel. The emitted flux integrated over the complete area of the accretion disk is automatically conserved for the non-relativistic limit by using the chosen approach with the Cunningham transfer function (see, Cunningham, 1975; Dauser et al., 2010; Speith et al., 1995). Relativistic effects alter the observed flux in the expected way, by Doppler boosting and general relativistic red-shift. In addition to these effects the inclination to the accretion disk also plays an important role here. The intensity due to the projection on the sky follows roughly  $\cos \theta_{\text{obs}}$ . Relativistic light-bending slightly changes the picture. Especially the flux behind the black hole (as seen from the observer) is enhanced for large inclination angles.

The `relxilllp` model now returns this reflected flux together with the direct radiation from the primary source, which is given by Eq. 2.

### 3.2 The High Energy Cutoff

Besides the reflection fraction, measuring the high energy cutoff  $E_{\text{cut}}$  of the primary power law also allows to constrain the accretion geometry. Its value is strongly connected to the temperature of the corona, which also allows to draw conclusions about its size and origin. Especially since the launch of *NuSTAR* (Harrison et al., 2013), several good measurements of  $E_{\text{cut}}$  have been obtained (see, e.g., Ballantyne et al., 2014; Brenneman et al., 2014). However, as the *NuSTAR* energy range is 3–79 keV, constraining the high energy cutoff using the direct measurement of the continuum radiation only works up to 200 keV. As has been shown in García et al. (2015), remarkably the relativistic reflection is easily capable in constraining the cutoff energy up to 1000 keV. This is due to the fact that the cutoff of the primary spectrum has a distinct effect on the reflection spectrum around the Compton hump (20–40 keV) and also at energies below 10 keV.

García et al. (2015) show in explicit simulations the capabilities to constrain the cutoff with the reflection method. Additionally it is shown that only applying the cutoff on top of the reflection spectrum yields poor and systematically biased results. Therefore using the cutoff as built in by `xillver` and `relxill` is essential for accurate results. A main conclusion of the aforementioned publication is that while only *NuSTAR* data can only set constraints when  $E_{\text{cut}} < 400$  keV. Combined datasets, e.g., by adding *Suzaku* to the *NuSTAR* data, allows to constrain the energy of the cutoff of 1 mCrab sources far beyond the energy range of the detectors. The highly increased sensitivity below 10 keV is responsible for this effect and clearly demonstrates the impact of the cutoff energy on the complete reflection spectrum.

Using now the `relxill` setup, additional information of the source in terms of height/compactness and reflection strength can be obtained from the same data. A systematic study of these parameters will allow us to draw firmer conclusions on the geometry of the source and test coronal models. The main challenge for those models is to predict the huge amount of flux emitted at the compact primary sources, which are found from timing (reverberation) and spectral (relativistic reflection) measurements.

## 4 Summary and Conclusions

Relativistic reflection is a complicated interplay between irradiation, the reflection in the rest frame of the disk, and the smearing of the reflected spectrum on its way to the observer. Besides the spectrum also intensities strongly change. Especially strong reflection features are created by compact primary sources, which irradiate an accretion disk around a rapidly rotating black hole. The newest version of the `relxill` model does incorporate all of these effects. By choosing the lamp post geometry it is possible to directly fit intrinsically the irradiating source. The characterizing parameter is the reflection fraction, which is defined

by the ratio between photons emitted towards the disk and towards the observer.

Additionally we motivated that the high energy cutoff of the direct radiation can be measured indirectly by fitting relativistic reflection. It was shown that for values far beyond the observed energy band strong constraints can be put on  $E_{\text{cut}}$  (García et al., 2015). Especially good results are obtained when combining high energy data from *NuSTAR* with detectors at lower energies, such as *Suzaku*.

Having now tools at hand for directly analyzing the geometry of the accreting systems, a systematic study of these objects and their properties are the next important step for understanding the extremes of the accretion at the smallest scales.

*Acknowledgements.* This research has made use of ISIS functions provided by ECAP/Remeis observatory and MIT (<http://www.sternwarte.uni-erlangen.de/isis/>). We gratefully thank John E. Davis for developing the `SLXFIG` module, which was used to prepare all figures in this publication.

## References

- Ballantyne D.R., Bollenbacher J.M., Brenneman L.W., et al., 2014, *ApJ* 794, 62
- Barr P., White N.E., Page C.G., 1985, *MNRAS* 216, 65P
- Bautista M.A., Kallman T.R., 2001, *ApJS* 134, 139
- Brenneman L.W., Madejski G., Fuerst F., et al., 2014, *ApJ* 781, 83
- Brenneman L.W., Reynolds C.S., 2006, *ApJ* 652, 1028
- Cackett E.M., Zoghbi A., Reynolds C., et al., 2014, *MNRAS* 438, 2980
- Cunningham C.T., 1975, *ApJ* 202, 788
- Dauser T., García J., Parker M., et al., 2014, *MNRAS* 444, L100
- Dauser T., García J., Wilms J., et al., 2013, *MNRAS* 687
- Dauser T., Svoboda J., Schartel N., et al., 2012, *MNRAS* 422, 1914
- Dauser T., Wilms J., Reynolds C.S., Brenneman L.W., 2010, *MNRAS* 409, 1534
- Dovčiak M., Karas V., Yaqoob T., 2004, *ApJ Suppl.* 153, 205
- Duro R., Dauser T., Wilms J., et al., 2011, *A&A* 533, L3
- Fabian A.C., Miniutti G., Gallo L., et al., 2004, *MNRAS* 353, 1071
- Fabian A.C., Parker M.L., Wilkins D.R., et al., 2014, *MNRAS* 439, 2307
- Fabian A.C., Rees M.J., Stella L., White N.E., 1989, *MNRAS* 238, 729
- Fabian A.C., Vaughan S., 2003, *MNRAS* 340, L28
- Fabian A.C., Zoghbi A., Ross R.R., et al., 2009, *Nat* 459, 540
- García J., Dauser T., Lohfink A., et al., 2014, *ApJ* 782, 76
- García J., Dauser T., Reynolds C.S., et al., 2013, *ApJ* 768, 146
- García J., Kallman T.R., 2010, *ApJ* 718, 695
- García J., Kallman T.R., Mushotzky R.F., 2011, *ApJ* 731, 131
- García J.A., Dauser T., Steiner J.F., et al., 2015, *Astrophys. J., Lett.* 808, L37
- Guainazzi M., Bianchi S., Dovčiak M., 2006, *Astron. Nachr.* 327, 1032
- Harrison F.A., Craig W.W., Christensen F.E., et al., 2013, *ApJ* 770, 103
- Kara E., Fabian A.C., Cackett E.M., et al., 2013, *MNRAS* 434, 1129
- Laor A., 1991, *ApJ* 376, 90
- Longinotti A.L., de La Calle I., Bianchi S., et al., 2008, *Mem. Soc. Astron. Ital.* 79, 259
- Marinucci A., Matt G., Miniutti G., et al., 2014, *ApJ* 787, 83
- Matt G., Perola G.C., Piro L., 1991, *A&A* 247, 25
- Matt G., Perola G.C., Piro L., Stella L., 1992, *A&A* 257, 63
- Miller J.M., Parker M.L., Fuerst F., et al., 2013a, *Astrophys. J., Lett.* 779, L2
- Miller J.M., Parker M.L., Fuerst F., et al., 2013b, *Astrophys. J., Lett.* 775, L45
- Miller J.M., Reynolds C.S., Fabian A.C., et al., 2008, *ApJ* 679, L113
- Mushotzky R.F., Done C., Pounds K.A., 1993, *ARA&A* 31, 717
- Nandra K., O'Neill P.M., George I.M., Reeves J.N., 2007, *MNRAS* 382, 194
- Nandra K., Pounds K.A., Stewart G.C., et al., 1989, *MNRAS* 236, 39P
- Patrick A.R., Reeves J.N., Porquet D., et al., 2011, *MNRAS* 411, 2353
- Pounds K.A., Nandra K., Stewart G.C., et al., 1990, *Nat* 344, 132
- Reis R.C., Fabian A.C., Ross R.R., et al., 2008, *MNRAS* 387, 1489
- Risaliti G., Harrison F.A., Madsen K.K., et al., 2013, *Nat* 494, 449
- Ross R.R., Fabian A.C., 2005, *MNRAS* 358, 211
- Ross R.R., Fabian A.C., 2007, *MNRAS* 381, 1697
- Ross R.R., Fabian A.C., Young A.J., 1999, *MNRAS* 306, 461
- Shakura N.I., Sunyaev R.A., 1973, *A&A* 24, 337
- Speith R., Riffert H., Ruder H., 1995, *Comp. Phys. Commun.* 88, 109
- Stella L., 1990, *Nat* 344, 747
- Tanaka Y., Nandra K., Fabian A.C., et al., 1995, *Nat* 375, 659
- Tomsick J.A., Nowak M.A., Parker M., et al., 2014, *ApJ* 780, 78
- Uttley P., Cackett E.M., Fabian A.C., et al., 2014, *Nat* 507, 72
- Wilkins D.R., Fabian A.C., 2012, *MNRAS* 424, 1284
- Wilkins D.R., Gallo L.C., 2015, *MNRAS* 449, 129
- Wilms J., Reynolds C.S., Begelman M.C., et al., 2001, *MNRAS* 328, L27